A Report

entitled

ANALYTICAL STUDY OF TWIN-JET SHIELDING
SEMI-ANNUAL PROGRESS REPORT

NASA Grant No. NAG 1-11

Submitted by the

TEXAS A & M RESEARCH FOUNDATION

to

National Aeronautics and Space Administration
Langely Research Center

Prepared by

Dr. Carl H. Gerhold

of the

Department of Mechanical Engineering
Texas A & M University
College Station, Texas 77843

June 30, 1981

TABLE OF CONTENTS

Analytical Twin-Jet Shielding Study

I INTRODUCTION

The purpose of the project is two-fold. One task is development of the refined jet noise source model. The refinement of the noise source is expected to resolve discrepancies noted between previous analytical results with a point noise source model and experimental results for twin-jet shielding (1). The other task is comparison of the analytical model with experimental programs, sponsored by NASA-Langley. These experimental programs include shielding of a point noise source by a jet and twin jet shielding.

The progress reported to date is on development of the jet noise source model, and on comparison to experiments with the point noise source. The twin jet experimental program is in the development stage.

II JET NOISE MODEL

The estimated shielding of a point noise source compares favorably to twin-jet shielding measurements at locations near the jet axis (1). However, as the angle at which the incident sound impinging on the shielding jet increases, the point noise source model estimates greater shielding than is found experimentally. This is shown in Figure 1, where the ratio $\left|P_T/P_{in}\right|$ is the total (incident + scattered) far field sound pressure normalized by the incident sound pressure. It is felt that at locations nearly normal to the jet axis, the point source approximation of the jet noise source breaks down. In an effort to resolve this discrepancy it has been proposed to construct a more realistic noise source model to represent the far field noise emission from a jet.

A. Distributed Point Source Model

The proposal was to approximate the jet by a series of point noise sources

distributed along the jet axis, as shown in Figure 2. The magnitude of each source is a function of axial location as well as frequency. The results of experiments by Groshe (2) to measure the noise source distribution in a jet were investigated in order to obtain the axial distribution of source intensities. One such distribution, based on Groshe's experiments is shown in Figure 3. The figure shows the source distribution at 4000 H_z for a 20 mm diameter jet at nozzle exit Mach number of 1.0. The Strouhal number is .26. The source strength has been normalized by the maximum value. The distribution reaches a peak at approximately 7 diameters downstream, which corresponds to the end of the potential core. The source strength decreases downstream as well as upstream toward the jet. The far field sound pressure is evaluated from the relationship:

$$\underline{P}_{TOT} = \sum_{i=1}^{n} \frac{Q_i \, e^{ik_o R_i}}{R_i} \qquad (1)$$

where:

n = number of sources

Q_i = normalized source strength of the source

R_i = distance from the source to the receiver

k_o = wave number

The magnitude of $\underline{P}_{TOT}$ is plotted in Figure 4 as a function of angle in the plane of the jet axis. The magnitude of the sound pressure has been normalized by the magnitude of the peak sound pressure.

For the purposes of comparison, the experimentally obtained sound pressures based on measurements by Yu and Dosanjh (3) are shown in Figure 5. The directivity contours are from measurements on an 11.2 mm jet at Mach 1.5. The plots for 5000

(St = .12) and 20000 (St = .50) H_z are given to show the trend. The far field sound pressure contours are characterized by sharp peaks located between 25° and 30° from the jet axis, and rapidly diminishing values on either side of the peak.

Comparing Figure 4 to Figure 5, the source model does show a lobe at 30° from the jet axis. The sound pressure decreases rapidly as the jet axis is approached. At angles greater than 30°, the sound pressure first decreases as expected, but then increases to a peak value at 80° which is 13 times greater than the sound pressure at 30°. Thus it appears that, in addition to the magnitude distribution, a phase relationship exists among the sources.

B. Point Source Model with Imposed Directivity

While the analysis to date has not shown that the distributed point source model is invalid, the method appears to be limited in its applicability. Since the source is directional and the directionality is not readily obtained from the series of distributed point sources, a formulation is investigated in which directionality of the source is imposed. The far field sound pressure from a single source is:

$$\underline{P} = \frac{Q\,(\psi,\ f,\ M_j)\ e^{ik_o R}}{R} \tag{2}$$

where a form of Q suggested for further investigation is:

$$Q = \frac{1}{\left[\left(1 - \frac{\sin\psi}{\sin\psi_m}\right)^2 + \alpha\,(f,\ M_j)\right]^{5/2}} \tag{3}$$

ψ = angle measured from jet axis

ψ_m = angle at which the directivity is maximum

$$= \cos^{-1} \frac{\left(c_o/c_j\right)}{M_j}$$

α = coefficient which depends on the frequency and Mach number.

The form of expression for Q is suggested by Ribner's analytical work (4), emphasizing the convection of source noise downstream. The location of the maximum, ψ_m, is a strong function of the jet Mach number and the jet temperature. The term α serves largely to determine the relative strength of the source and is expected to be a strong function of frequency.

Equation 3 is tested by comparison to the curves in Figure 5. The conditions of the test are:

$M_j = 1.5$

$c_o/c_j = 1.30$

$\therefore \psi_m = 30.2^o$

Since the curves in Figure 5 are normalized by the peak, equation 3 is normalized to 1 at the peak, or,

$\alpha = 1.$

The normalized sound pressure curve is plotted in Figure 6. It is seen that the comparison with experimental data is sufficiently good to warrant further investigation of the imposed directivity point source model.

The model of a point source with directivity imposed by terms which depend on operating conditions of the jet is preferred for its simplicity. The model is readily incorporated into the existing shielding program.

III COMPARISON TO POINT SOURCE SHIELDING EXPERIMENTS

Measurements of the sound pressure level from a point source near a jet were made by Dr. J.C. Yu at NASA Langley Research Center. For the purposes of testing the analytical model, comparison of the measured shielding to the shielding estimated by the model are made.

The conditions of the test discussed in this report are:

1. Air jet
2. $T_o = T_j = 530.4^{\circ}R$
3. $M_j = 0.531$
4. $S/D = 2.5$
5. $k_o a = 0.56, 0.96, 1.6$

Figure 7 shows the definition of the terms used in the analysis. The angle ψ_n varies over a range from 0° (on the z-axis) to 120° (upstream of the source); and the angle θ varies from 0° (on the source side of the shielding jet) to 180° (on the side of the jet opposite the source).

Figure 8 is the normalized sound level in the shadow of the jet ($\theta = 180°$). In this figure the total sound pressure, P_{TOT}, is normalized by the incident sound pressure, P_{in}, and expressed as a normalized Sound Pressure Level, Δ SPL, where:

$$\Delta \text{ SPL} = 10 \log_{10} \left| \frac{P_{TOT}}{P_{in}} \right|^2$$

Thus, Δ SPL > 0 indicates amplification and Δ SPL < 0 indicates sound level reduction.

At values of $\psi_n > 90°$ (upstream of the noise source), the model correctly estimates that sound amplification occurs. The model underestimates the magnitude of this amplification by as much as 2.5 dB. In the downstream region, the model estimates the trend of increasing sound level reduction with increasing frequency. However, the model estimates a more gradual rate of sound reduction than is

observed as the jet axis is approached. Moreover, the model underestimates the magnitude of the Δ SPL, with the discrepancy increasing not only as the jet axis is approached but as frequency increases.

The azimuthal variation of the normalized Sound Pressure Level is plotted at two planes downstream of the source in Figure 9 through 14. Figure 9 through 11 are plotted at $\psi_n = 30°$ for normalized frequencies, $k_o a = 0.56, 0.96, 1.6$. Figures 12 through 14 are plotted at $\psi_n = 60°$ for each of the three frequencies.

From Figures 9 through 11, the model estimates the trend of the distribution in sound level; with backscattering decreasing and sound concentrating into a lobe adjacent to the shadow zone as frequency increases. The model underestimates the backscattering at low frequency (Figure 9); but follows the measured values in the shadow zone. In the middle frequency (Figure 10), agreement is good except near the value of maximum sound reduction. At high frequency (Figure 11), the model underestimates the maximum noise reduction. The model generally follows the trend of measured data at high frequency except near $\theta = 0°$ where the receiver is on the source side of the jet. The model shows a lobe of backscattering which is 4 dB higher than that observed experimentally. Both the model and the experiment indicate that the sound level is reduced at $\theta = 0°$.

Figures 12 through 14 show that at $\psi_n = 60°$ the model estimates the correct trend of the data and generally, the analytical result is within ± 2 dB of the measured value. The major discrepancy is seen at $k_o a = 1.6$ (Figure 14). At this high frequency the experimental data show a stronger peak in the lobe adjacent to the shadow zone and also that the shadow zone is not as broad as the model estimates.

Comparison at other values of ψ_n shows that the general trend is for good agreement between the experiment and the model for ψ_n large. As the jet axis is approached, discrepancies increase, not only with decreasing ψ_n, but also with increasing frequency. The disagreement between the model and experiment is most critical at points where the normalized sound pressure indicates maximum amplification or reduction.

The effect of downstream distance on width of the shadow zone is demonstrated in Figure 15. The angle β is the included angle of the shadow zone; that is, the zone on the side of the jet opposite the source in which the normalized sound pressure level is less than 0.0. The model shows two trends; one that the shadow zone becomes narrower as the frequency increases and the other that the shadow zone becomes broader as the jet axis is approached.

The trend for the shadow zone to become narrower as the frequency increases is consistent with the results of analysis of the 2-dimensional model (5). The relationship between the included angle and the frequency from the previous analysis is:

$$\beta = 2.2\ (k_o S)^{-.37} \quad \text{(rad)} \tag{4}$$

where:

S = the spacing between the jet and the source.

The limiting values of β from the above relationship are shown at $\psi_n = 90°$ on Figure 15. The values at $\psi_n = 90°$ agree with the included angles from the 2-dimensional analysis to within 0.25 radians.

The measured data exhibit the narrowing of the shadow zone with increasing frequency at locations near the jet axis. The trend of the data is not consistent at receiver locations nearly normal to the jet axis.

From equation 4, it is also seen that the shielding zone is expected to become narrower with increasing source/jet separation. This result is consistent with barrier theory. However, the curves in Figure 15 indicate that as the angle of incidence goes farther away from normal, (the source/shielding jet separation effectively increases), the shadow zone becomes broader. The trend toward a broader shadow zone as the effective separation increases is unexpected, based on barrier theory and previous analysis. However, the measured data on Figure 15 exhibit this trend and are in general agreement with the model.

IV ACTION REQUIRED

A. Noise Source Development

Further work on the jet noise model which consists of a point source with directivity imposed is required. Far field jet noise experiments with subsonic and supersonic jets will be investigated in order to refine the directivity model.

The jet noise model will be included in the jet shielding model and the analytical results compared with experimental results reported in the literature. Comparison will also be made with experimental results obtained by United Technologies Research Center in a parallel twin jet shielding program.

B. Comparison to Experimental Data

The comparison of the analytical model to experiments with twin jet shielding was discussed in the previous paragraph.

In addition, more extensive comparison to point source shielding experiments by NASA-Langley personnel will be made. Data which is presently being analysed is for a Mach number 0.886 unheated air jet and for a subsonic, simulated hot air jet using helium. The purpose of such comparison is to resolve discrepancies between the measured shielding and the estimated shielding which are noted as the jet axis is approached, and to suggest any necessary refinements of the shielding jet model. The comparison also will serve to define more completely the mechanisms of shielding.

REFERENCES

1. Gerhold, C.H., "Analytical Study of Twin-Jet Shielding - Final Report" Report for NASA Grant # NAG-1-11. December 31, 1980.

2. Groshe, F.R., "Distributions of Sound Source Intensities in Subsonic and Supersonic Jets", AGARD Conference Proceedings No. 131 on Noise Mechanisms.

3. Yu, J.C. and Dosanjh, D.S., "Noise Field of Coaxial Interacting Supersonic Jet Flaws", AIAA paper no. 71-152, 1971.

4. Ribner, H.S., "The Issue of Source Terms for Jet Noise", Presented at 3rd AIAA Aero-Acoustics Conference - Palo Alto, CA. July 20-23, 1976, AIAA paper no. 76-487.

5. Gerhold, C.H., "Analytical Study of Twin-Jet Shielding - Two- Dimensional Model". Progress Report #2 for NASA Grant #NAG-1-11. July 1980

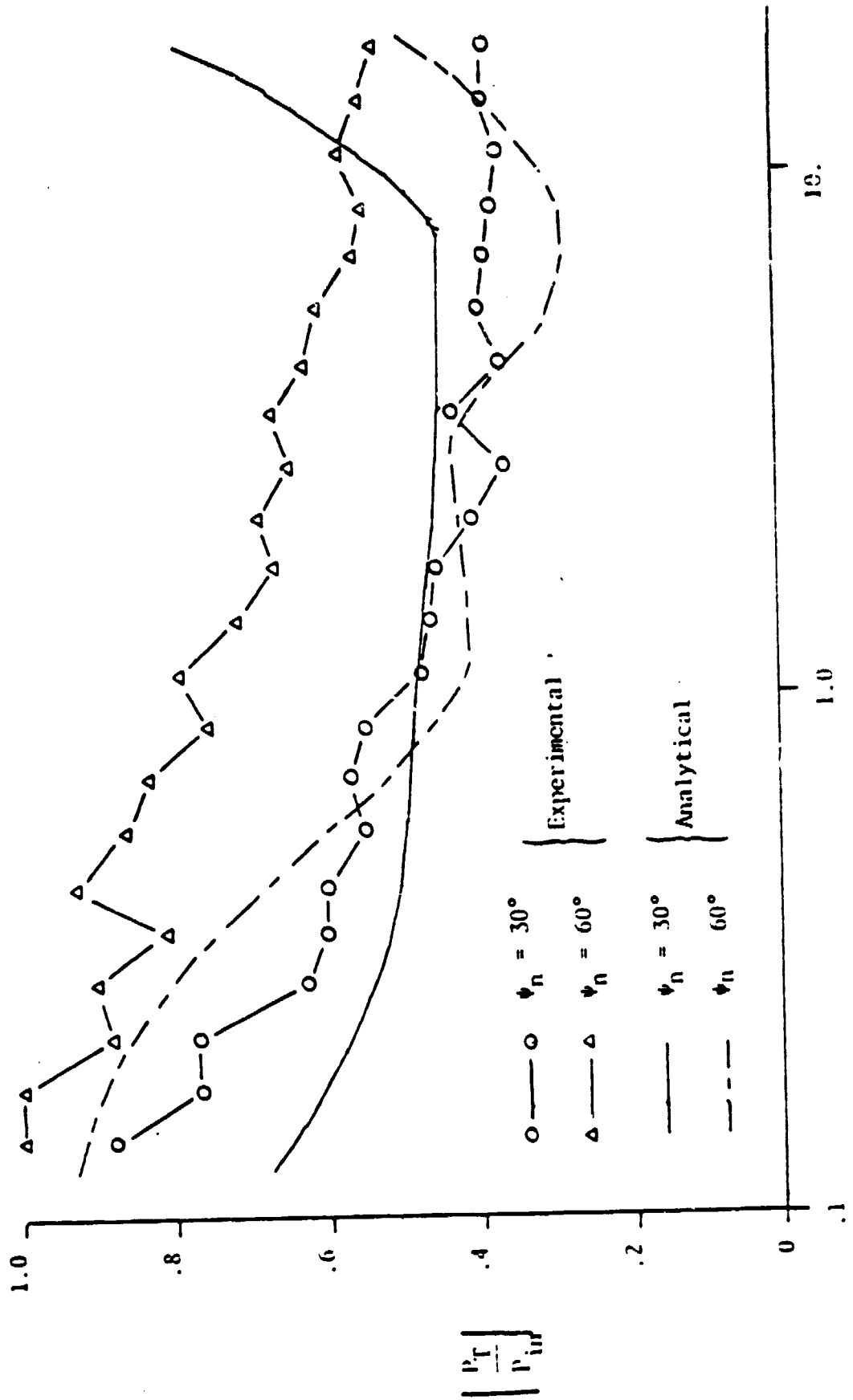

Figure 1 . Comparison of Analytical to Experimental Jet Shielding

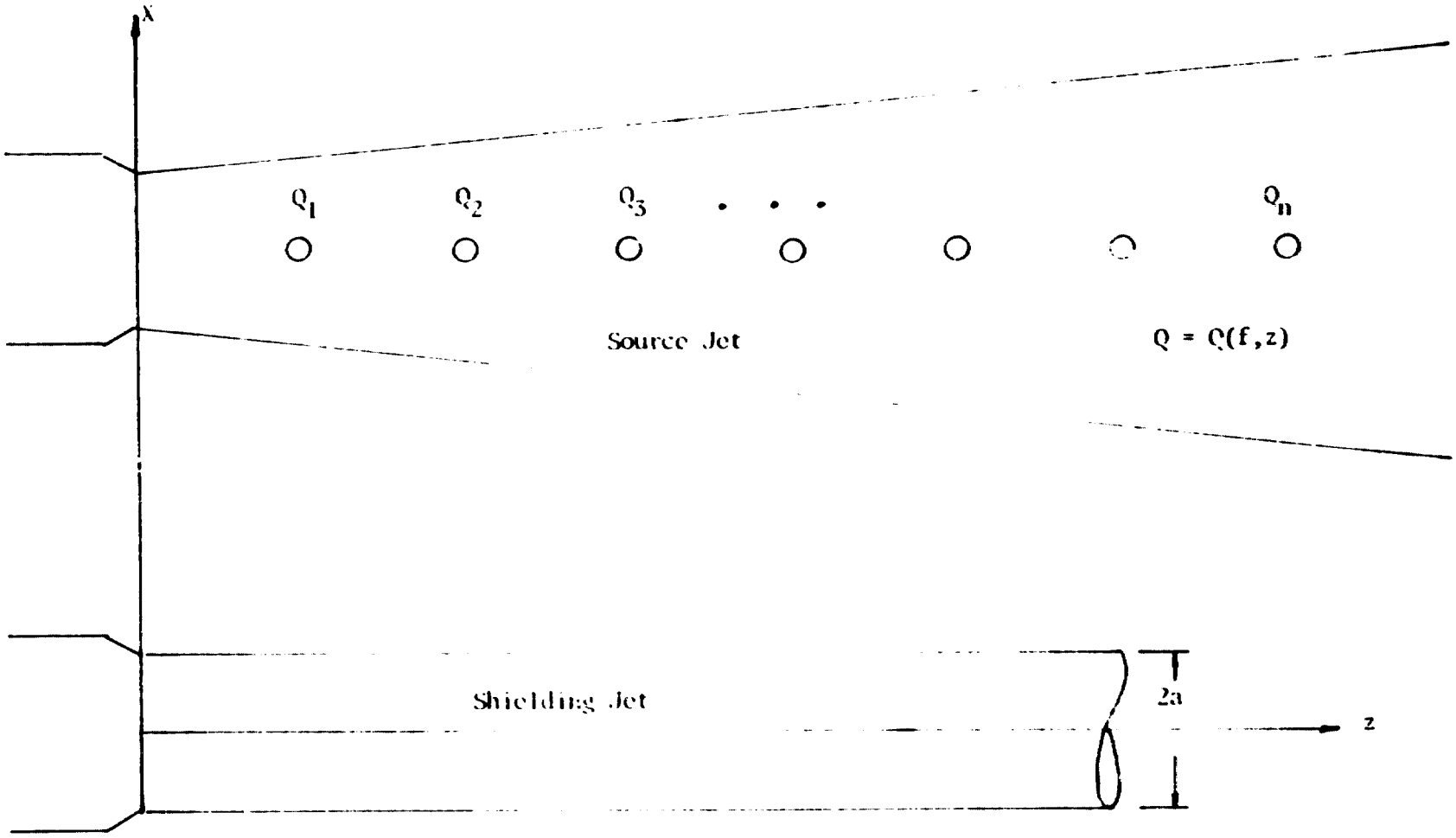

Figure 2. Representation of Distributed Point Noise Source Model for Source Jet Noise Simulation.

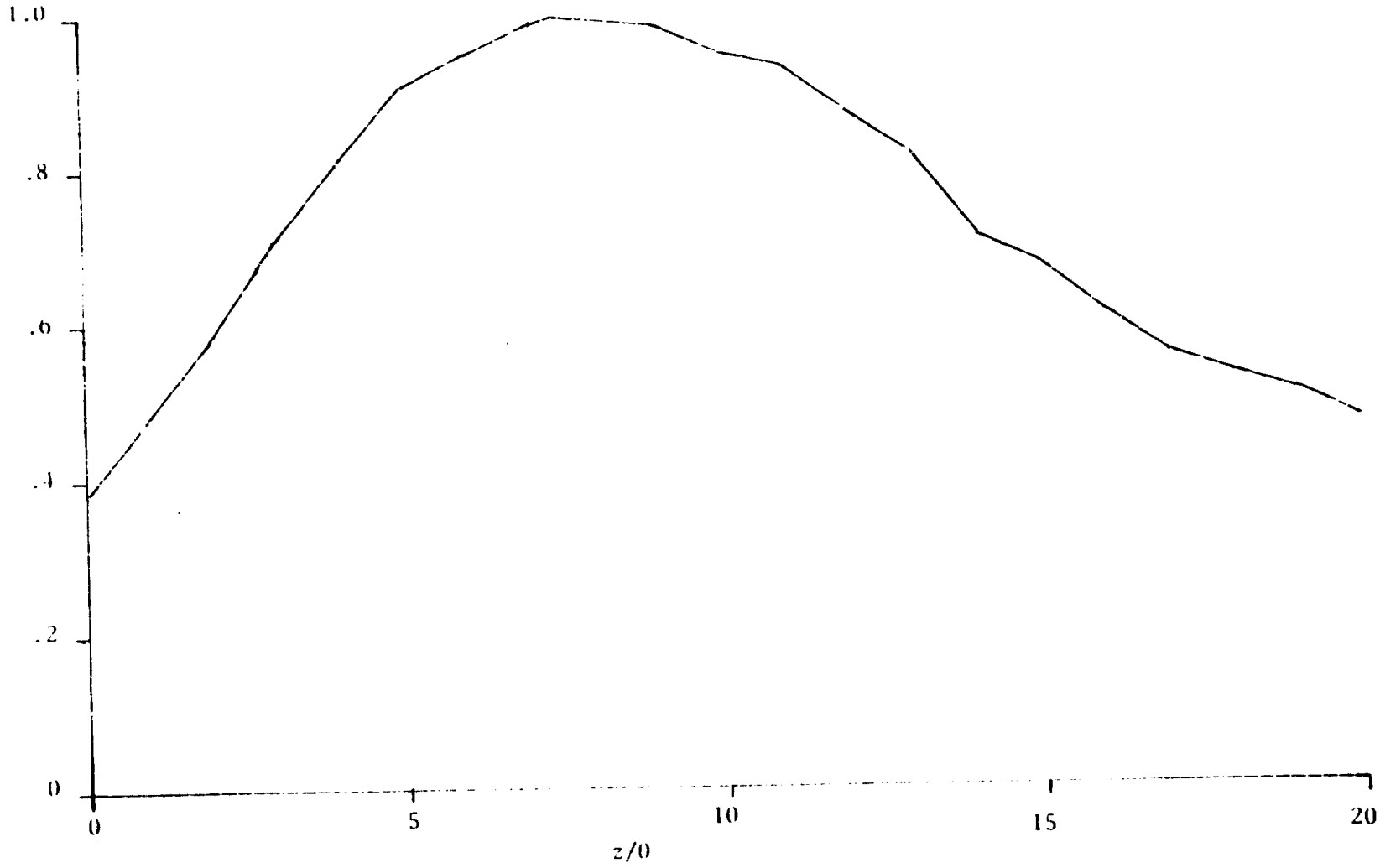

Figure 3. Source Distribution for Point Source Series Approximation of Jet Source (based on ref.2)

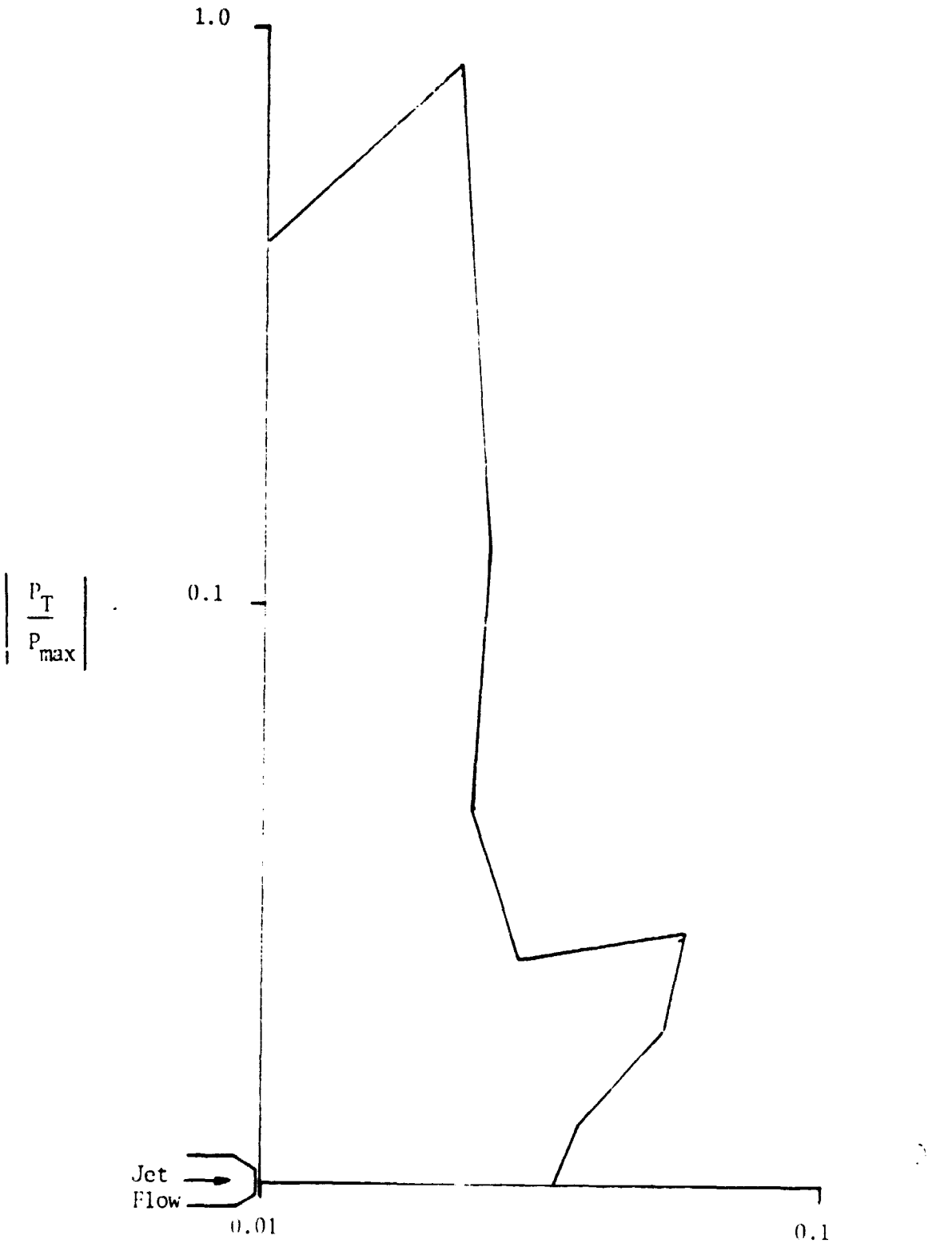

Figure 4. Radial Distribution of Far Field Sound Pressure based on Distributed Point Source Model.

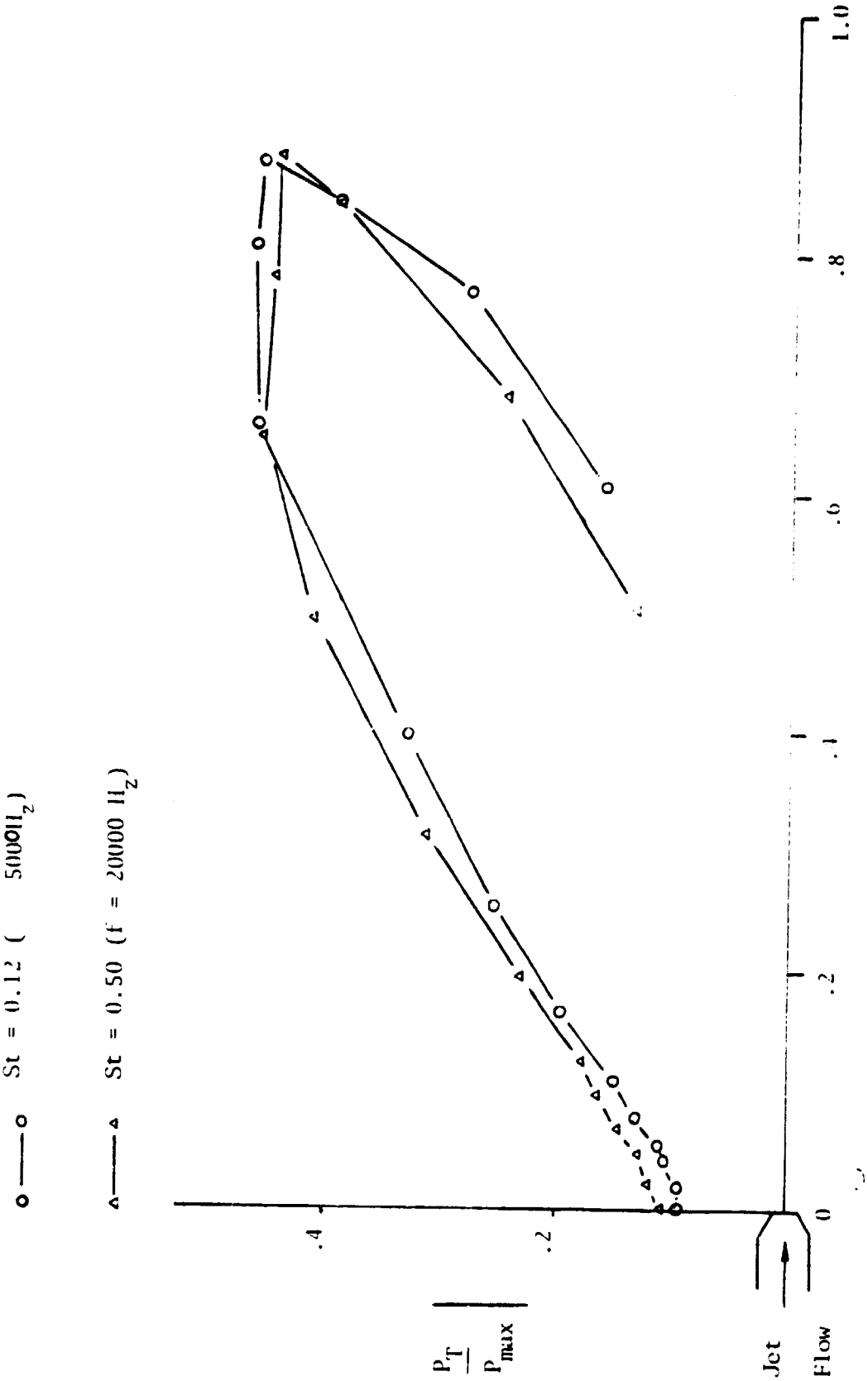

Figure 5. Radial Distribution of Far Field Normalized Sound Pressure for Unheated Supersonic Jet (ref. 3)

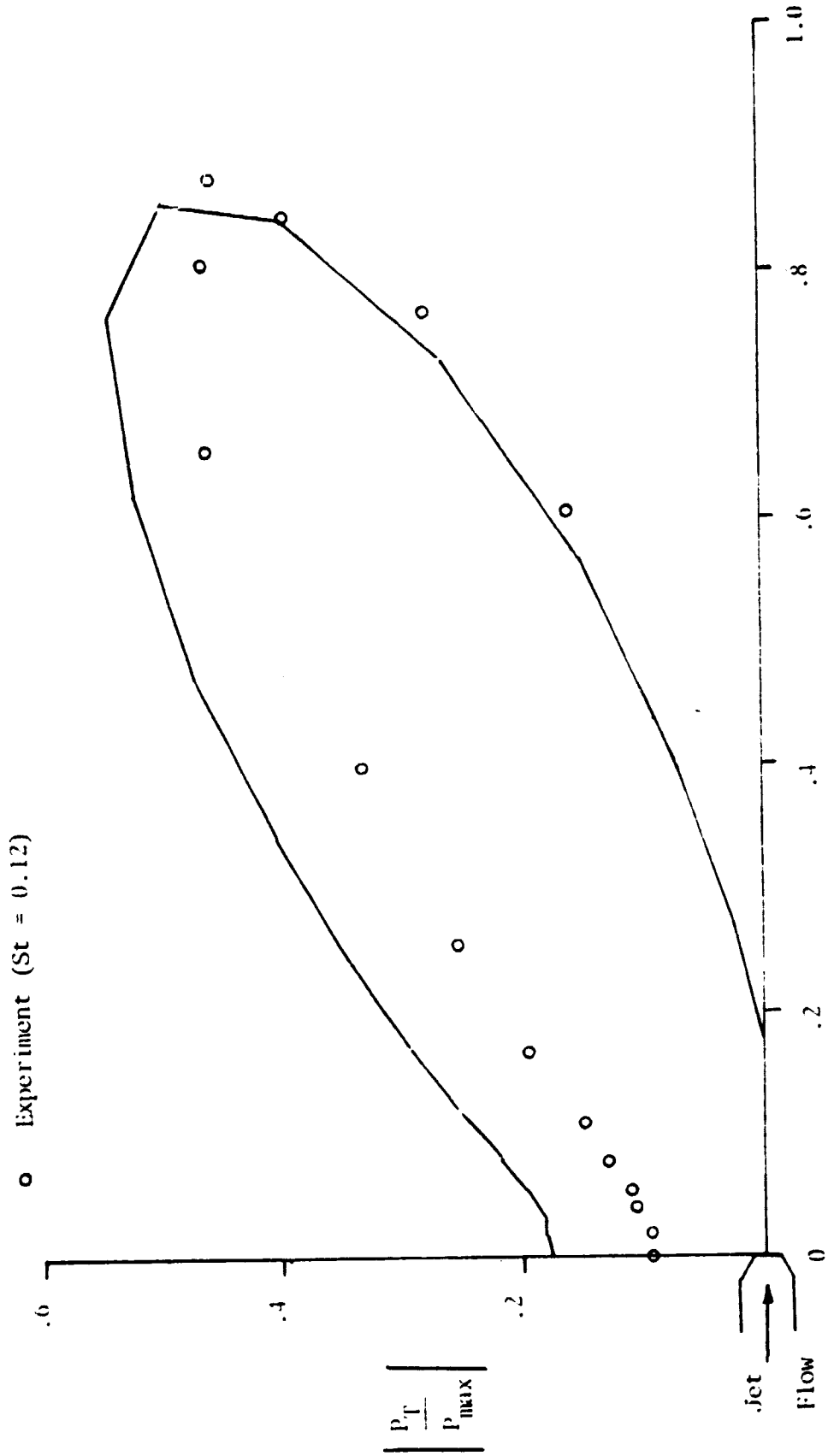

Figure 6. Radial Distribution of Normalized Far Field Sound Pressure based on Source Model with Directivity Function.

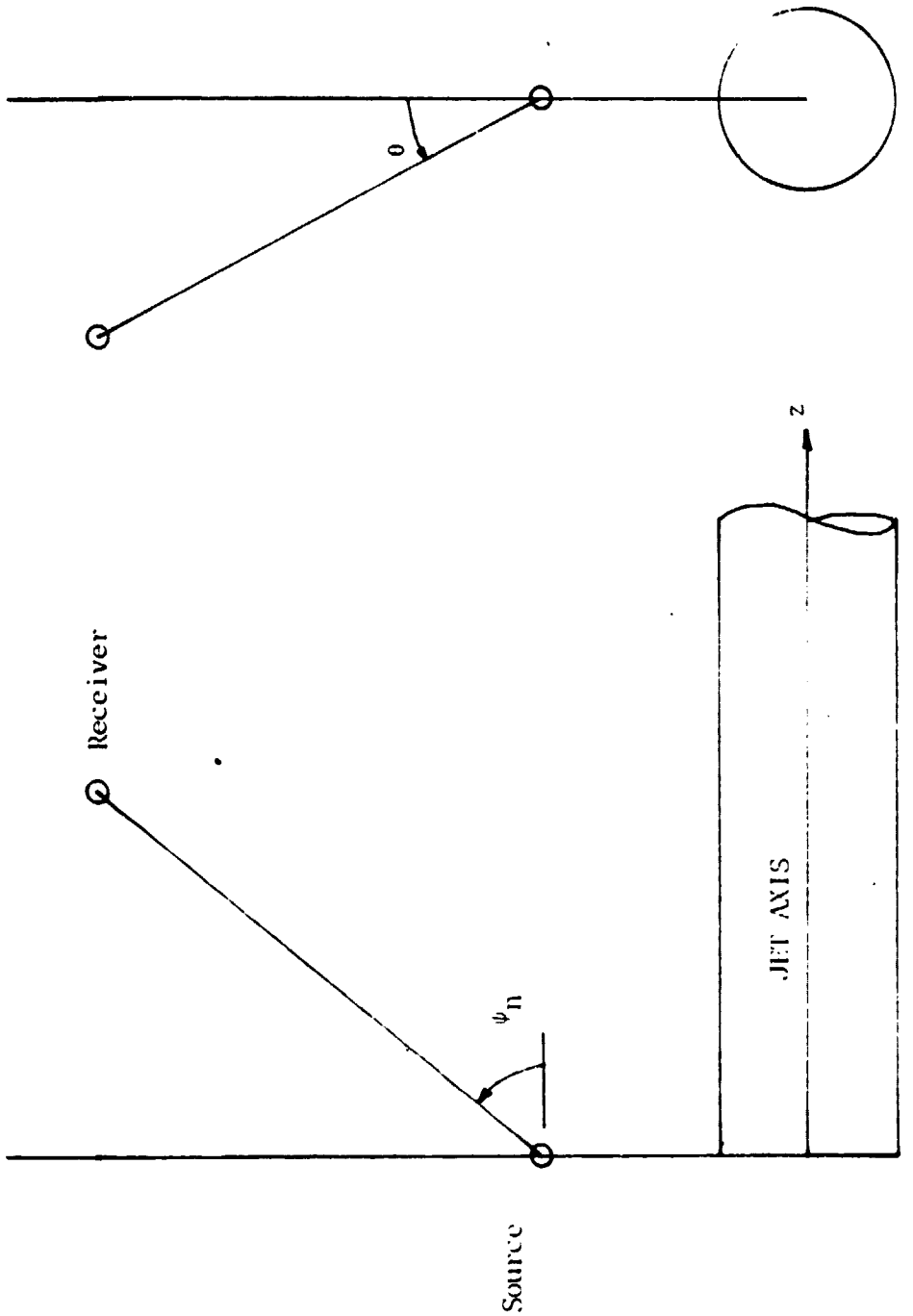

Figure 7. Representation of Angles Used in Analysis of Jet Shielding

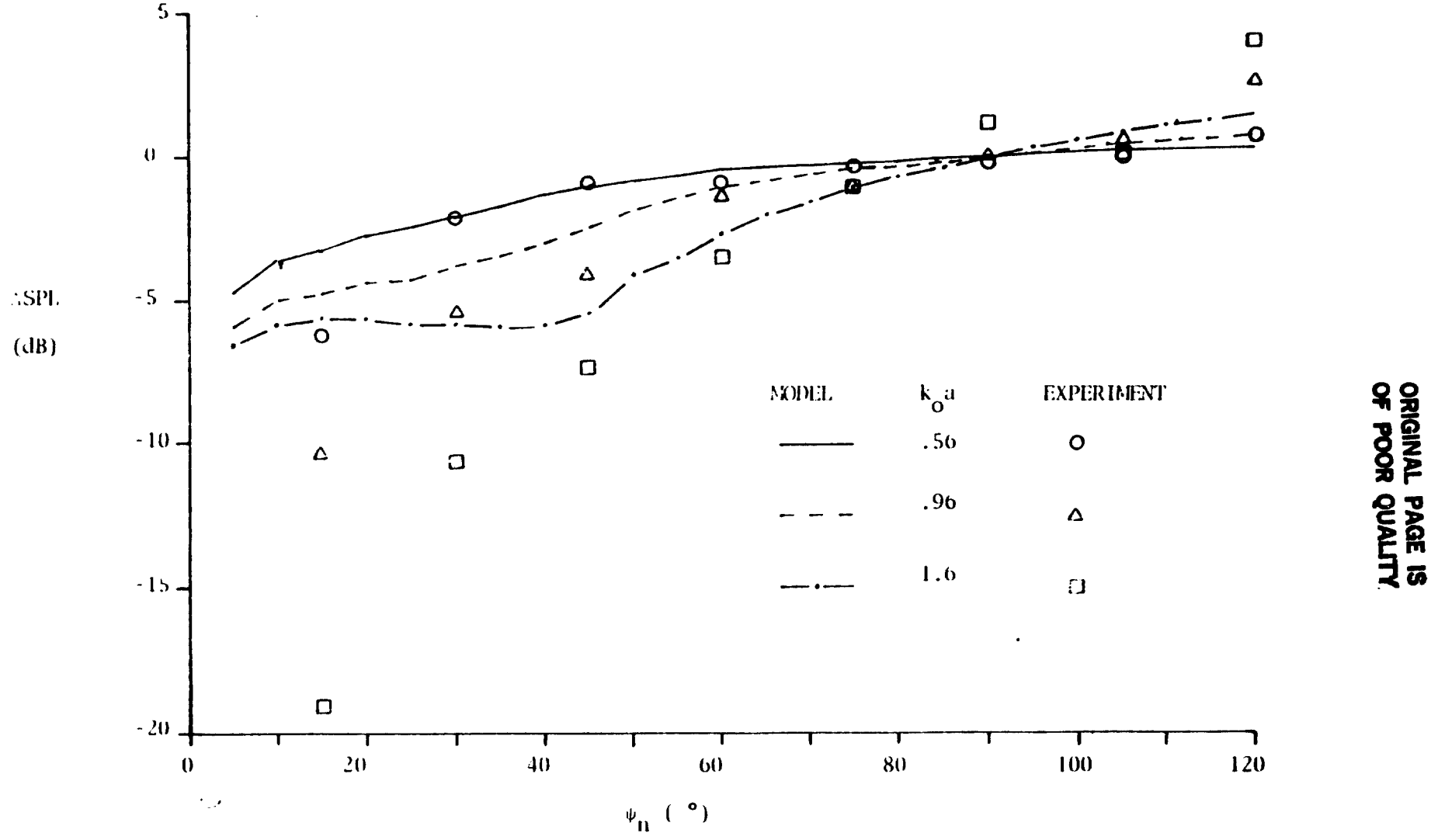

Figure 8. Normalized Sound Pressure Level in Shadow Zone. Air Jet, T_0/T_j = 1.0, M_j = 0.531

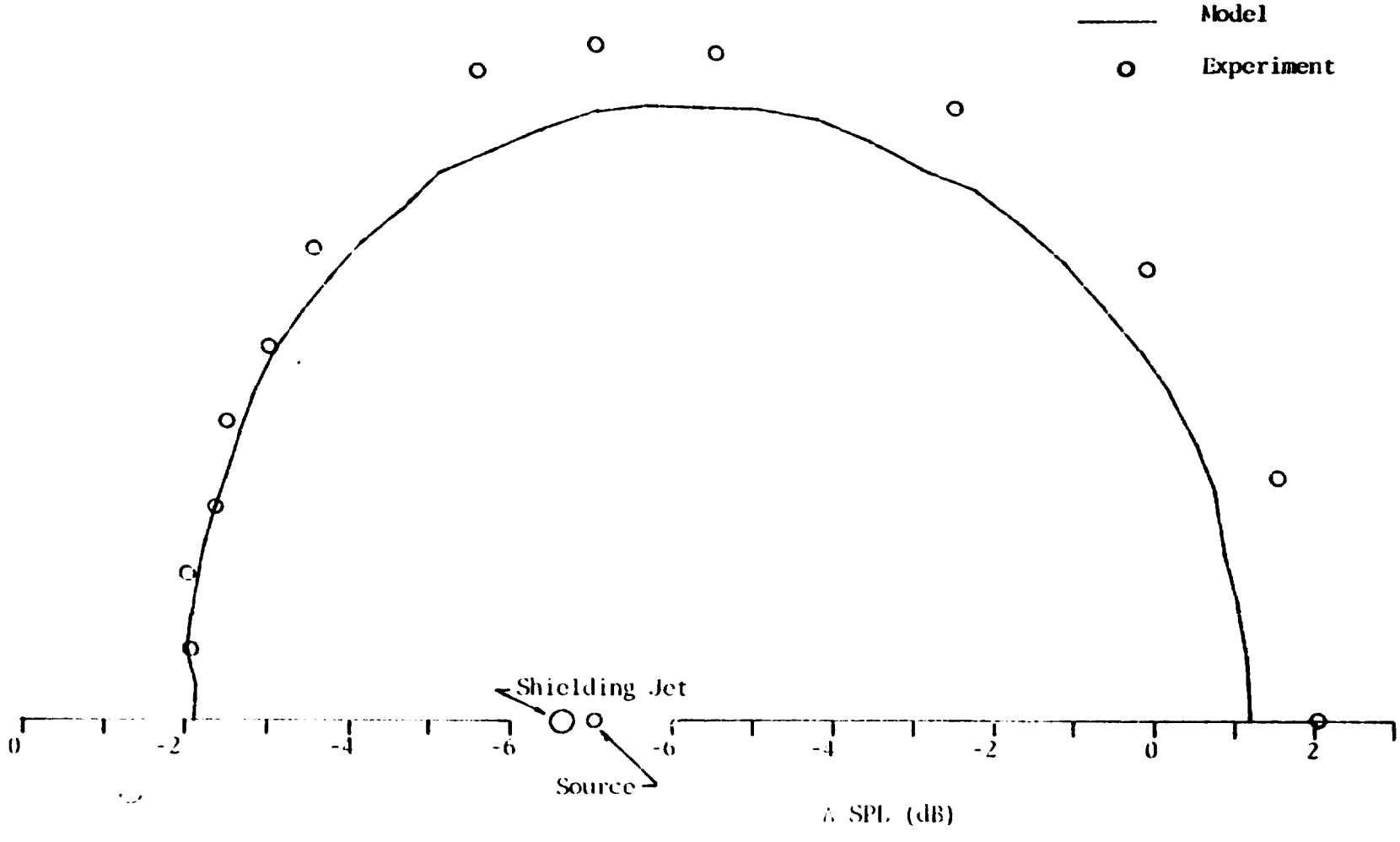

Figure 9. Azimuthal Variation of Normalized Sound Pressure Level. Air Jet = $\psi_n = 30°$, $k_o a = 0.56$

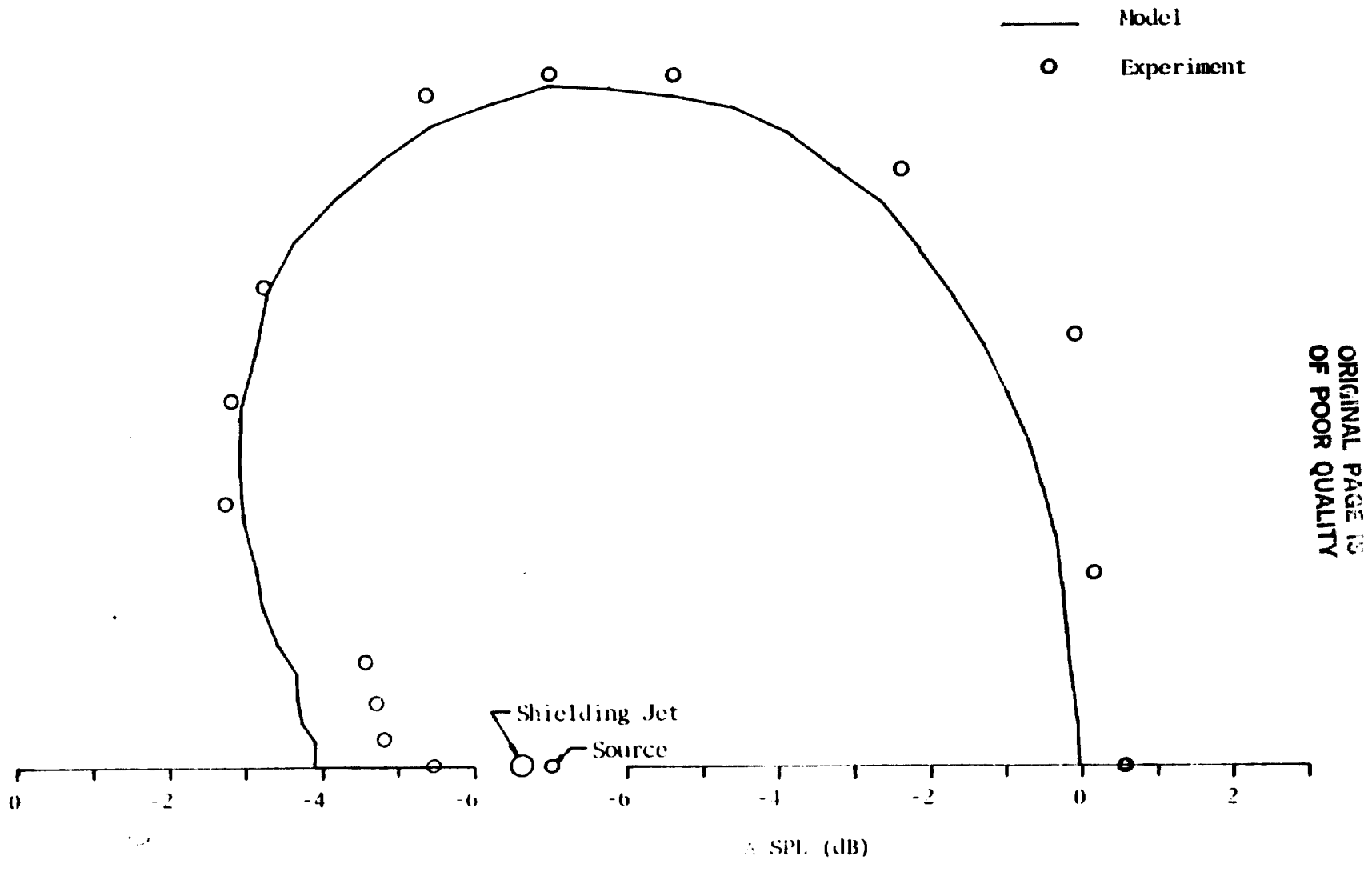

Figure 10. Azimuthal Variation of Normalized Sound Pressure Level. Air Jet, $\psi_n = 30°$, $k_o a = 0.96$

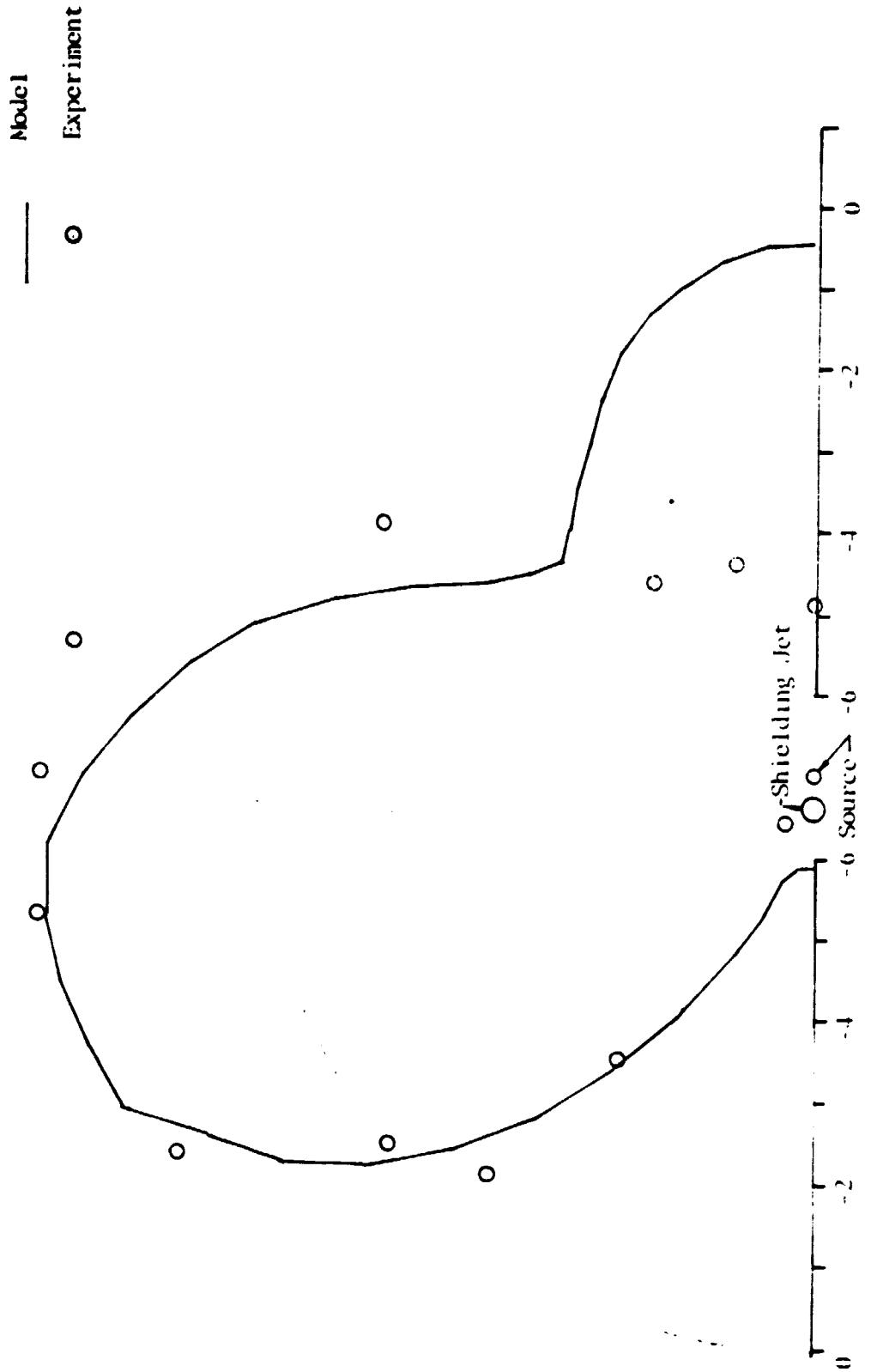

Figure 11. Azimuthal Variation of Normalized Sound Pressure Level. Air Jet, $\psi_n = 30°$, $k_0 a = 1.6$

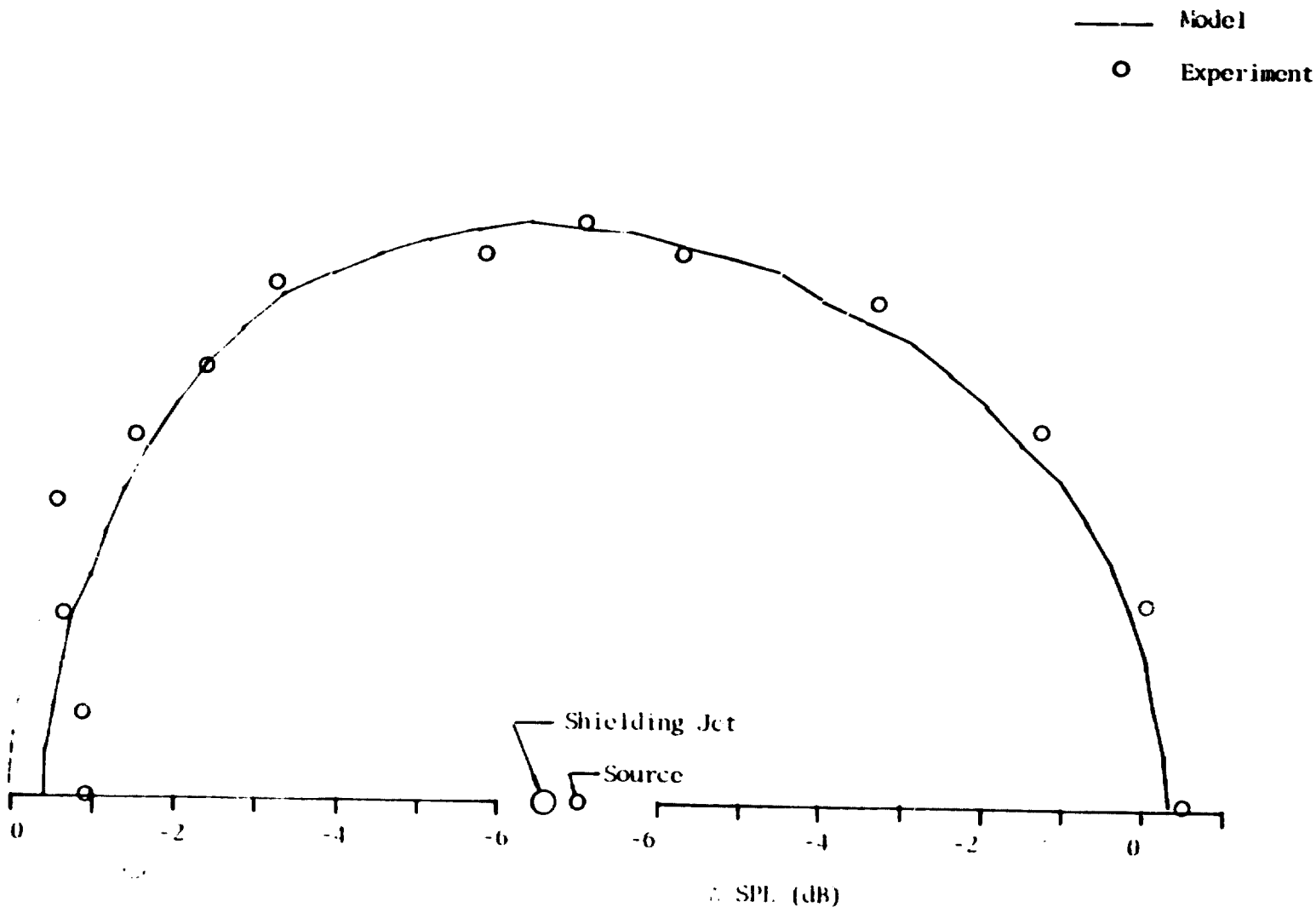

Figure 12. Azimuthal Variation of Normalized Sound Pressure Level. Air Jet, $\psi_n = 60°$, $k_o a = .56$

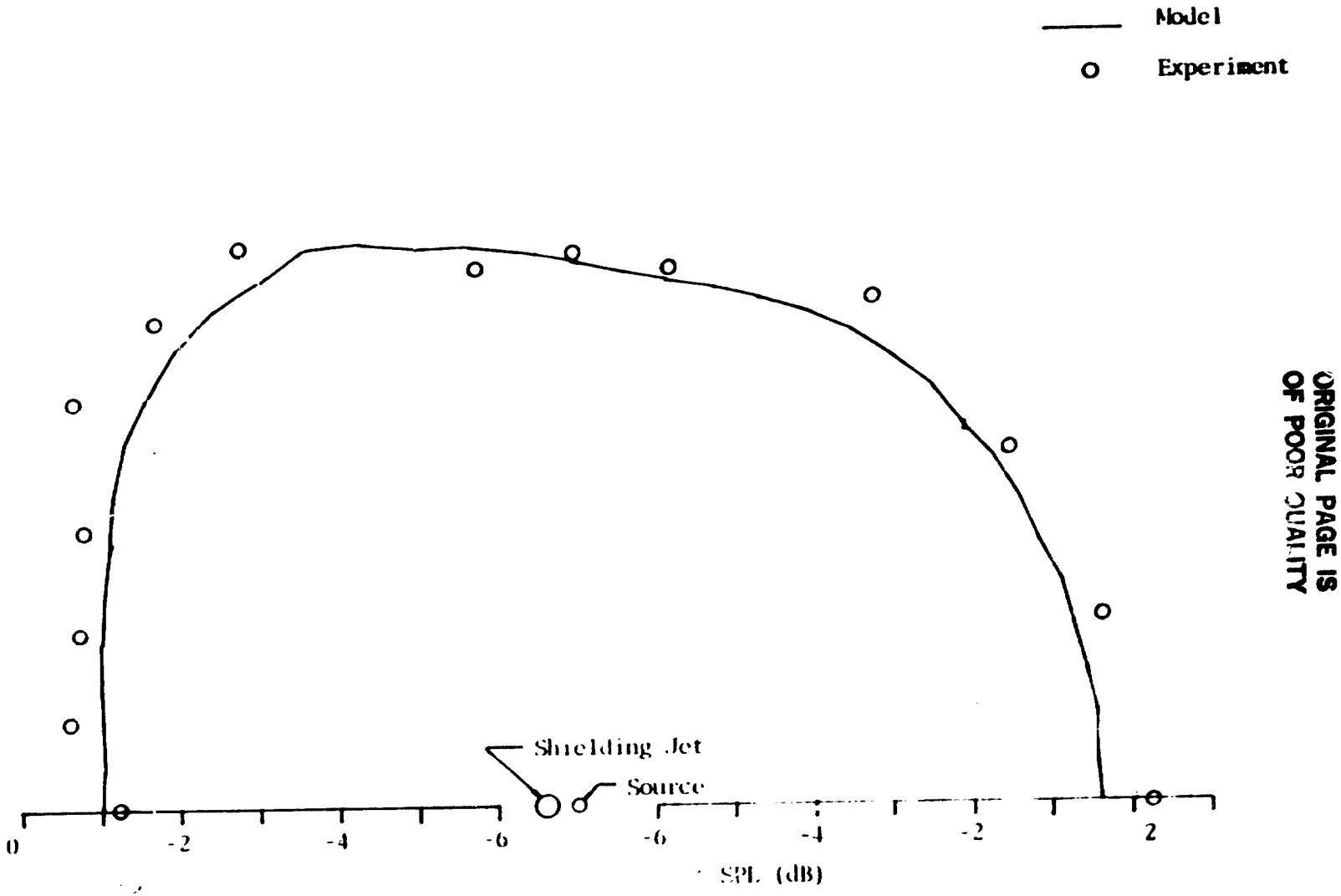

Figure 13. Azimuthal Variation of Normalized Sound Pressure Level. Air Jet, $\psi_n = 60°$, $k_s a = .96$

Figure 14. Azimuthal Variation of Normalized Sound Pressure Level. Air Jet, $\psi_n = 60°$, $k_o a = 1.6$

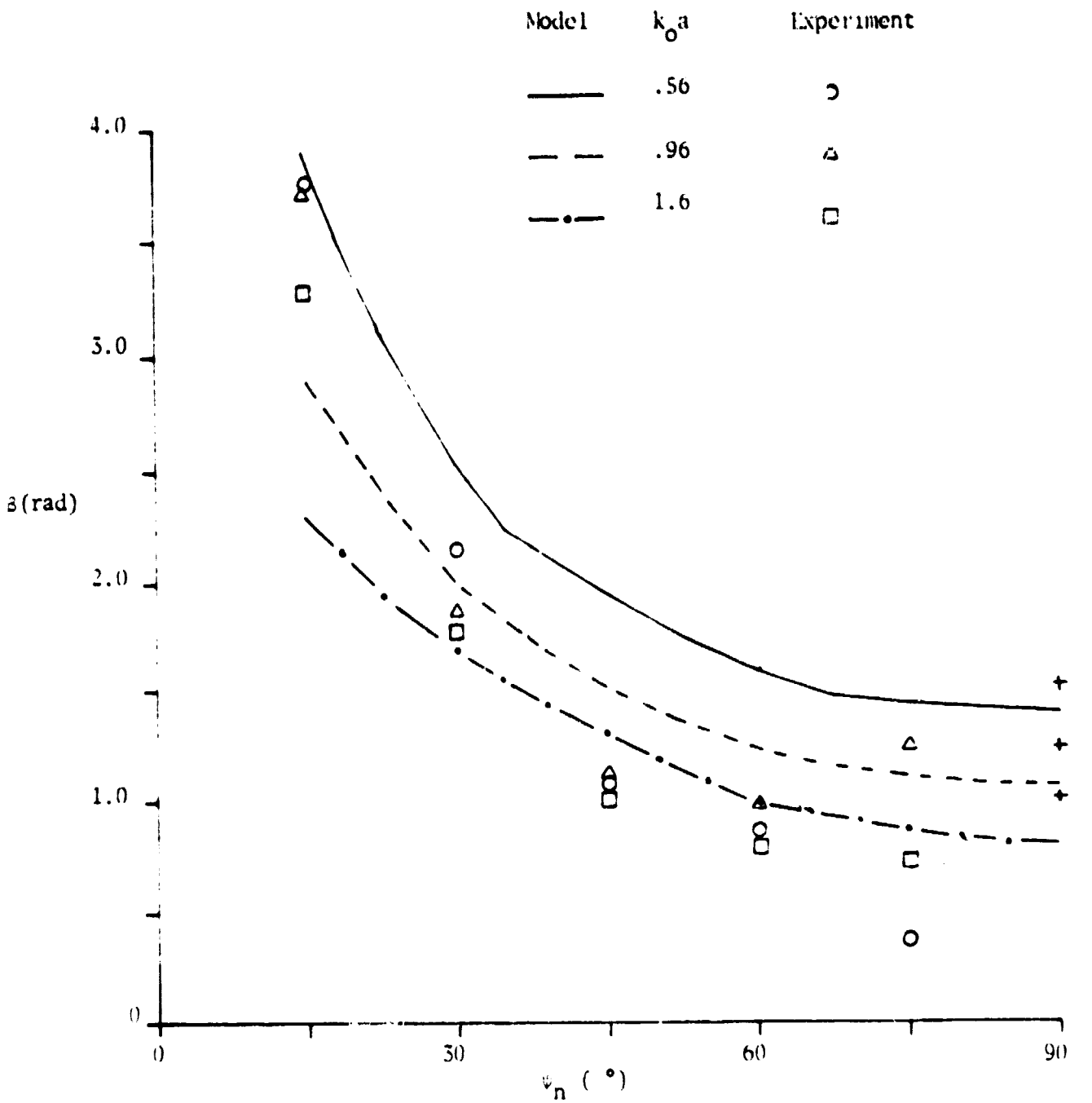

Figure 15. Shadow Zone Width, Air Jet, T_o/T_j = 1.0, M_j = 0.551

Note: marks at ψ_n = 90° are estimated from 2-dimensional analysis.